An Analysis of TIMS Imagery for the Identification of Manmade Objects

Daniel K. Gordon, Paul W. Mueller, and *Matthew Heric*
Autometric, Incorporated, 5301 Shawnee Road, Alexandria, VA 22312

ABSTRACT: Night-time data acquired by the NASA Thermal Infrared Multispectral Scanner (TIMS) have been analyzed to evaluate the potential for discriminating and identifying manmade objects based on their thermal infrared (TIR) signatures. After processing the data with a decorrelation stretch, it was possible to distinguish several types of metal- and stone-covered roofs based on their compositional differences. The distinctions between these roofs were not evident in broad-band TIR imagery simulated from the TIMS data. These preliminary results indicate that a multispectral TIR capability may have considerable value in reconnaissance sensor packages such as Aided Target Recognition (ATR) systems.

INTRODUCTION, BACKGROUND, AND OBJECTIVES

Aided Target Recognition (ATR) systems promise to enhance significantly the effectiveness of reconnaissance systems by reducing operator workload while increasing operational speed. Problems exist, however, in the processing and analysis of sensor-derived information.

One problem identified with current ATR testbeds is high false-alarm rates. False-alarms occur when unique combinations of object descriptors cannot be identified. Measurements of object descriptors can be made in three domains: spectral, spatial, and temporal. Currently, many ATR systems employ Forward Looking Infrared (FLIR) sensors, which collect imagery with a single band in the 8- to 12-μm region. Radiative temperature differences between terrain elements can be observed using both day- and night-time imagery acquired with the FLIR sensors. However, broad-band thermal infrared (TIR) measurement cannot detect the wavelength-dependent emissivity differences which exist between terrain materials.

The TIR region contains emission minima generated by specific molecular or crystalline bonds, such as Si-O in quartz. Exploitation of the spectral features in the TIR requires a multispectral capability. A series of investigations have documented the utility of multispectral TIR data for the discrimination and identification of rock and soil compositions based on the wavelength positions of emission minima (e.g., Gillespie *et al.*, 1986). An extensive review of the physics and optics of thermal infrared remote sensing for the geological and biophysical sciences can be found in Putnam (1986) and Schott (1989). The Putnam work also provides an exhaustive bibliography of thermal infrared research and basic information for related disciplines.

In this preliminary investigation we examine the differentiation of several manmade objects using night data acquired with the NASA Thermal Infrared Multispectral Scanner (TIMS). Utilization of the visible and NIR regions is severely constrained during night-time surveys. Thus, our objective is to explore the utility of developing a multispectral TIR capability for real-time reconnaissance applications, which could be used under night conditions. Such a system would have advantages over the current broad-band TIR sensors if it (1) reduced the number of false-alarms in ATR systems; and (2) provided spectral signatures for identifying the composition of natural and manmade objects present in terrain elements.

METHODS

ACQUISITION AND ORGANIZATION OF THE IMAGERY

The data analyzed in this study were collected by the NASA Thermal Infrared Multispectral Scanner, or TIMS, in six bands located in the 8.2- to 11.7-micrometre region of the electromagnetic spectrum. The characteristics of the TIMS system are given in Table 1. TIMS data were collected on the night of 29 April 1986, at approximately 2:00 a.m. (local) over Little Rock Air Force Base using the NASA Lear jet. The data had a nominal spatial resolution of 3.4 metres. The area selected contained buildings and other manmade objects. The digital imagery analyzed consisted of a 512- by 512-pixel subscene extracted from the original data set. There were a number of bad scanlines found in band 5 of the data set; therefore, this band was not used in the enhancement part of the study.

Supporting reference data utilized for this project included NASA Thematic Mapper Simulator (TMS) imagery, color infrared 9-inch format aerial photography (scale = 1:6600), and various maps of the study site. These reference data were accessed for interpreting the TIMS imagery and identifying the features of interest.

ENHANCEMENT OF THE IMAGERY

The five TIMS bands utilized in this study tended to be very highly correlated. When bands are so highly correlated, the data are redundant, meaning that brightness measurements for several bands are quite similar. Inspection of the images showed some distinctive differences, yet a method was needed to reduce correlation and enhance the TIMS imagery. The method selected was the decorrelation-stretch technique (Gillespie *et al.*, 1986) which has been applied successfully in previous studies (Soha and Schwartz, 1978; Taylor, 1973). This method was augmented by processing the intermediate principal component images with spatial filters to reduce noise and improve the final images.

TABLE 1. THERMAL INFRARED MULTISPECTRAL SCANNER (TIMS) OPERATING PARAMETERS (ADAPTED FROM PALLUCONI AND MEEKS, 1985.)

Number of Channels:	6	
Spectral Ranges (full width at half maximum):		
	CH 1	8.2 - 8.6 μm
	CH 2	8.6 - 9.0 μm
	CH 3	9.0 - 9.4 μm
	CH 4	9.6 - 10.2 μm
	CH 5	10.3 - 11.1 μm
	CH 6	11.3 - 11.7 μm
Instantaneous Field of View:		2.5 mrad
Pixels per scan line:		638
Spatial resolution (@ 4500 feet altitude):		3.4 m
Detectors:		HgCdTe

PHOTOGRAMMETRIC ENGINEERING & REMOTE SENSING,
Vol. 57, No. 12, December 1991, pp. 1599–1604.

0099-1112/91/5712–1599$03.00/0

The decorrelation-stretch technique involved three steps. First, the Karhunen-Loeve (K-L) transform was applied to the data to obtain non-correlated principal component images. Next, the principal component images were contrast enhanced. For this study, the use of both a linear stretch and a Gaussian stretch was investigated. Last, the stretched principal component images were transformed back to the original measurement space using an inverse K-L transform.

The decorrelation-stretch technique allows the measurement space to be used much more effectively. Figure 1 illustrates the two-band case.

In Figure 1a, when pixel values for two bands are plotted against each other, the values fall in a linear alignment because the two spectral bands are highly correlated. The PC transformation rotates the coordinate space so that the first axis is along the direction of maximum variation and the second axis is orthogonal to this. Figure 1a shows the selection of new axes, and Figure 1b shows the data rotated into the new coordinate space. In Figure 1c a contrast stretch is applied to the data to utilize more of the measurement space. Finally, in Figure 1d the inverse transformation is applied to return to the original image coordinate (or measurement) space. When Figures 1a and 1d are compared, it can be seen that the measurement space is more fully utilized in the latter. Thus, spectral differences between targets are enhanced.

Median Filtering

In each case the last three principal component images were quite noisy. To reduce noise found in these images, a median filter was selected. Digital filters, such as the median filter, are arithmetic procedures that operate on a digital data set to remove irrelevant data or noise (Swain and Davis, 1978). Filtering can be done in one of two domains: the frequency-transform domain or the spatial domain (Gonzalez, 1986). The median filter operates in the spatial domain and, in turn, digital values of many adjacent image pixels are utilized to derive a new value for a particular pixel (usually central to the group). The image area considered in a single filtering operation is called the window.

The median filter is a non-linear operation in which the digital numbers within the window are ranked and the median or midvalue is selected. The window is moved over the entire image. The window size utilized in this research was 5 by 5. The 5 by 5 median filter was applied to the last three (of five) principal component images for the Little Rock data set.

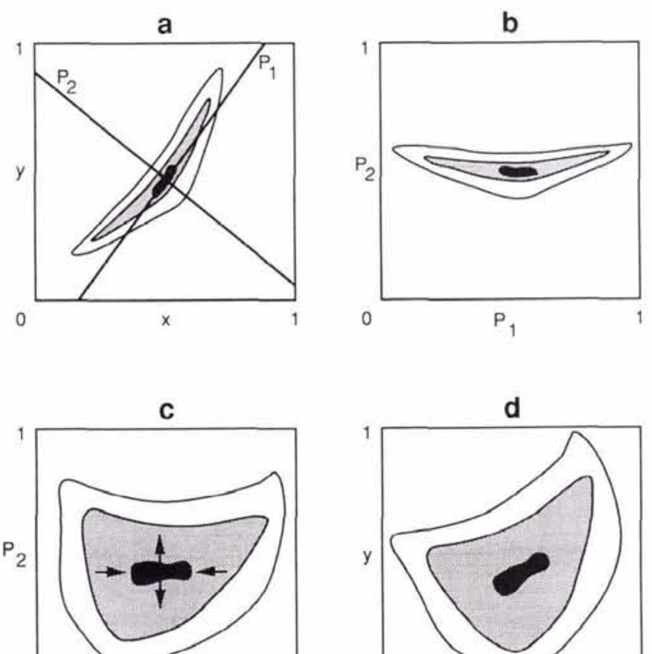

FIG. 1. Diagrammetric representation of the decorrelation-stretch technique applied to the study data. (a) Diagram of data (*X,Y*) as acquired and orthogonal principal axes P1 and P2. Zones surrounding the data represent standard deviations. (b) Data cluster after principal component transformation. (c) Linear contrast stretches applied to the "decorrelated" P1 and P2 channels. The arrows indicate the relative sense of expansion of the data to fill the data plane. (d) The stretched data returned to the *X,Y* coordinate system by the inverse transformation. The cluster now fills the plane (from Gillespie *et al.*, 1986).

Generation of Representative Statistics

For the purpose of determining the spectral properties of various features in the TIMS imagery, objects (mostly manmade) were selected using color infrared reference photography, and statistics were generated for these areas in the TIMS data. The TIMS imagery was displayed using a Gould DeAnza FD5000 image display and compared to the reference photography and maps. All objects large enough to be easily identified were noted, out of which several were selected representing a variety of materials. These objects were outlined by polygons which bounded the respective features of interest. The digital data for each polygon from the specified TIMS images were then extracted, and a variety of first-order statistics were generated. Six buildings having either gabled or flat rooftops were selected in the TIMS data set. The appearance of these objects in the color infrared photography was noted and first-order statistics were generated.

ATR systems are single-band (broad-band) sensors. Therefore, for comparison purposes, a broad-band image was created. A linear combination of the six original TIMS bands was made with each band equally weighted.

Principal Component Images

The first step in the decorrelation stretch was to generate principal component images. These images were linear combinations of five narrow-band thermal images (band 5 had too much noise to be used). Because a number of images were being combined, it was possible for the dynamic range of the output image to exceed that of the input images (in this case, 8 bits); therefore, the images were scaled. Normally, the scaling factor (gain) used to expand or compress the output image with the largest dynamic range (PC1) is applied to each of the bands so that the resultant five PC images are comparable in relative terms. When the same gain is applied to all PC images, the least significant PC images may have dynamic ranges of only 3 to 6 DN prior to stretching. Because the goal of the decorrelation-stretch was to enhance the contrast of the PC images, it was decided to apply variable gains to the PC images at the time they were generated, thus utilizing the full dynamic range available. The variable gain settings stretched the PC images so that the minimum and maximum values were scaled to 0 and 255. These images were then stretched further by saturating a percentage of pixels at the low and high ends, setting them to 0 and 255.

The weighting of each band when being combined to form principal component images was defined by an eigenvector. Eigenvectors defining each principal component are shown in Table 2, along with their eigenvalues. These eigenvalues were used to determine the information content of the various principal component images. For example, of all the information contained in the five TIMS bands being analyzed in this section,

TABLE 2. LITTLE ROCK: EIGENVECTORS, EIGENVALUES, AND AMOUNT OF VARIATION ACCOUNTED FOR BY EACH PRINCIPAL COMPONENT IMAGE

	PC1	PC2	PC3	PC4	PC5	Eigen-values	% Variation
BAND1	−0.3230	0.3888	0.1209	−0.6944	−0.4978	55.8	92.6
BAND2	−0.2829	0.3840	−0.0015	−0.2564	0.8407	40.9	6.74
BAND3	−0.3088	0.6098	−0.4118	0.5650	−0.2109	4.6	0.75
BAND4	−0.5561	−0.1102	0.7461	0.3480	−0.0293	1.6	0.27
BAND6	−0.6411	−0.5635	−0.5091	−0.1109	0.0070	0.8	0.14

92.1 percent of the total amount of variance in the data set was contained in the first PC image and only 0.14 percent in the last PC image. For data reduction purposes, the last band or least significant band is normally dropped, which in this case would reduce the amount of data by 20 percent and reduce the information content of the data set by one-tenth of a percent.

This would be a questionable act even though the least significant PC images were noisy and contained small amounts of information. Although sample sizes were small, from earlier analyses it was determined that LR3 (a stone-covered roof) was not distinguishable from LR4 (a metal roof) in the broad-band or any of the narrow-band TIMS imagery, but LR3 and LR4 were separable in PC4 with means of 86.4 and 114.99 and standard deviations of 6.16 and 5.13, respectively (Table 3). This was true even though PC4 accounted for less than 0.3 percent of the total amount of information in the data set.

DECORRELATION STRETCH IMAGES

After the PC images were generated and stretched, an inverse Karhunen-Loeve (K-L) tranformation was applied to return the enhanced imagery to its original coordinate system. The effect of the enhanced noise in the PC images was apparent in the inverse transformed image. To reduce the speckling effect, a median filter was applied to the three least significant PC images. The resultant images were blurry but did not have the speckle associated with the non-filtered images. The PC images were then used in the inverse K-L transformation, improving results substantially.

The statistics resulting from the decorrelation-stretch and from the broad-band image are shown in Table 4. Analysis of the original TIMS imagery and the simulated broad-band image showed that, although there was confusion between different materials in the broad-band image, most of the confusion was eliminated when the narrow-band TIMS imagery was examined. One area of confusion did remain; LR3 (a stone-covered roof) and LR4 (a metal roof). In the decorrelation stretch imagery this area of confusion was eliminated in band 1 where LR3 had a mean and standard deviation of 94.45 and 4.11, respectively, and LR4 had a mean and standard deviation of 66.38 and 4.98, respectively.

TABLE 3. LITTLE ROCK: STATISTICAL MEANS AND STANDARD DEVIATIONS FROM TRAINING AREAS IN THE BROAD-BAND IMAGE AND THE PRINCIPAL COMPONENT IMAGES

		PC1	PC2	PC3	PC4	PC5	Broad-Band
LR1*	MEAN:	108.46	78.00	139.80	79.03	149.57	143.06
	STD:	6.22	11.9	11.04	5.43	6.75	6.31
LR2	MEAN:	186.03	121.37	182.64	134.87	140.56	69.31
	STD:	4.20	4.42	9.49	9.22	8.43	4.14
LR3*	MEAN:	119.01	65.18	139.69	86.42	160.66	132.26
	STD:	5.79	11.25	9.52	6.16	8.95	5.85
LR4*	MEAN:	122.44	42.00	153.70	114.99	165.76	127.77
	STD:	5.39	11.91	7.45	5.13	8.37	5.62
LR5*	MEAN:	105.77	154.94	100.33	131.83	192.48	148.08
	STD:	4.82	3.91	10.37	11.37	7.48	4.71
LR7	MEAN:	167.66	125.04	167.85	213.74	216.12	86.91
	STD:	7.42	6.77	12.39	8.56	8.66	7.41

* Targets with overlapping brightness values at ±2 standard deviations

TABLE 4. LITTLE ROCK: STATISTICAL MEANS AND STANDARD DEVIATIONS FROM THE BROAD-BAND IMAGE AND THE IMAGES RESULTING FROM THE INVERSE TRANSFORMATION OF THE STRETCHED AND FILTERED IMAGES

		1	2	3	4	6	Broad-Band
LR1*	MEAN:	105.94	99.29	36.66	167.66	117.77	143.06
	STD:	4.45	3.58	5.93	5.04	4.62	6.31
LR2	MEAN:	62.40	64.74	73.88	195.78	31.78	69.31
	STD:	3.27	4.83	4.95	3.74	3.95	4.14
LR3*	MEAN:	94.45	101.38	24.96	162.07	208.09	132.26
	STD:	4.11	4.90	6.17	6.23	4.83	5.85
LR4*	MEAN:	66.38	95.18	33.11	182.94	99.38	127.77
	STD:	4.98	5.16	6.57	6.12	5.46	5.62
LR5*	MEAN:	55.21	170.54	132.35	160.17	83.65	124.08
	STD:	11.37	4.54	8.16	7.20	6.94	4.71
LR7	MEAN:	5.34	158.39	63.53	188.69	37.18	86.91
	STD:	2.92	3.27	6.25	3.30	6.01	7.41

* Targets with overlapping brightness values at ±2 standard deviations.

RESULTS AND DISCUSSION

CORRELATION REDUCTION

The decorrelation-stretch technique was found to reduce greatly the correlation between the five TIMS bands (as previously noted, band 5 was not used due to noise). This was verified both visually and statistically. Plate 1 shows two color composite images. The left image (Plate 1a) is a combination of the original TIMS bands 6, 3, and 2 (blue, green, and red, respectively). Note that there is some coloration; however, much of the image is comprised of gray shades. This indicates that the brightness values of the three bands are quite similar (i.e., correlated). This right image (Plate 1b) is a color composite of the same three TIMS bands after undergoing the decorrelation-stretch process. There is a much greater range of colors, thus indicating that the decorrelation between the bands has been reduced. Several of the building roofs which appeared similarly in the original image composite, have quite different appearances in the enhanced image. Therefore, spectral differentiation of the buildings has been increased.

This reduction in correlation was also verified statistically. Table 5 shows the correlation matrices for the original five TIMS bands utilized, the principal component images, and the decorrelation-stretched images. It can be seen that correlation between bands has been reduced. This is beneficial if any statistical classification of the data is to be done, because the statistical separation between materials is increased.

STATISTICAL ANALYSIS

The statistical means and standard deviations generated for the test areas (six buildings) are shown in Table 6 for the original TIMS bands and the simulated broad-band image. To identify definitively any one of the targets spectrally, the brightness of the target, which is expressed by the digital number(s) (DN), must be unique. To identify an object with 95 percent confidence, there could be no overlap in the region defined by the mean ±2 standard deviations. In the broad-band image no target was free of overlap from all other targets and, therefore, could not be identified uniquely. The six targets clustered in two areas centered around a DN of 137 (i.e., LR1, LR3, LR4, and

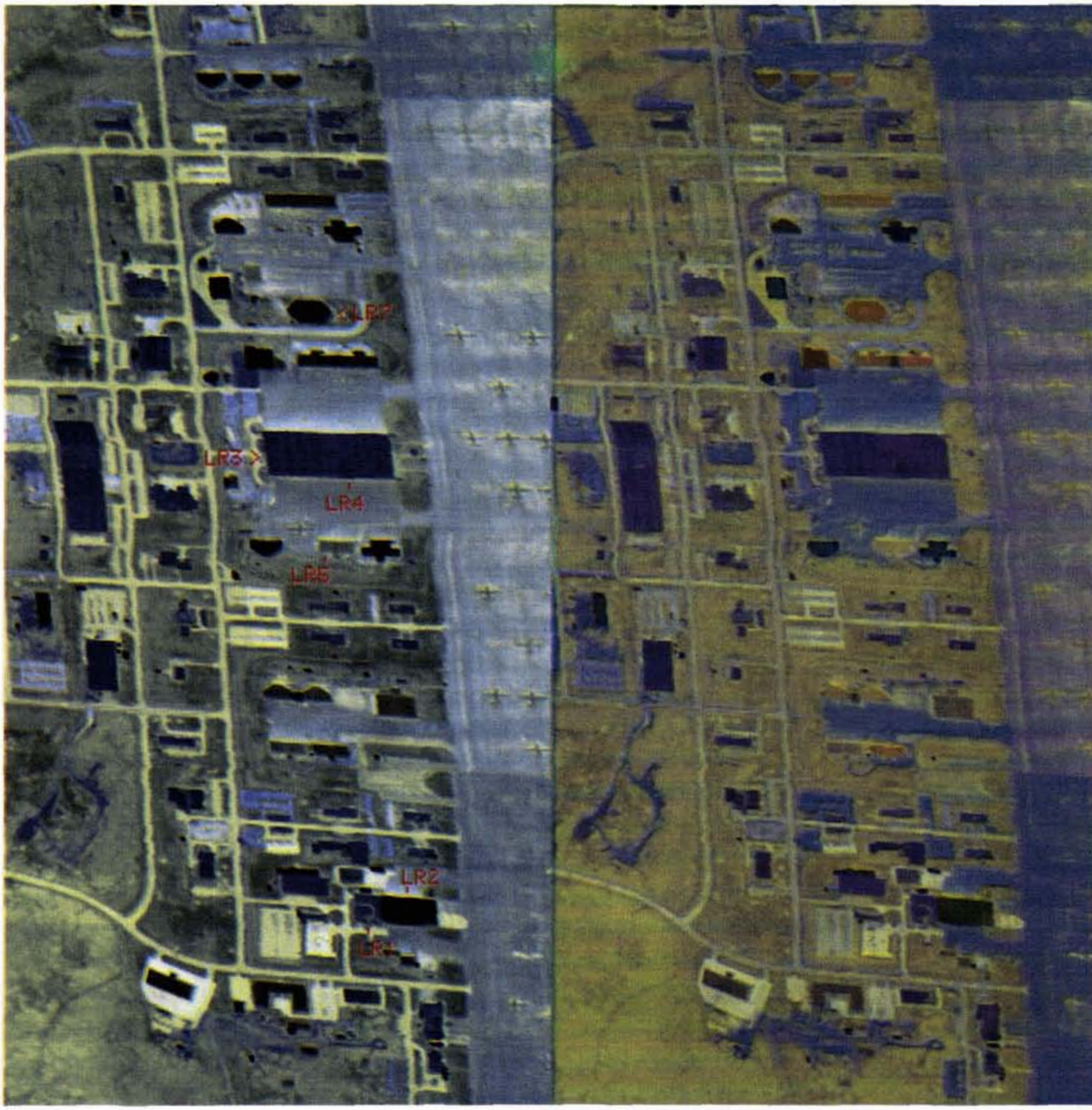

PLATE 1. Little Rock: Comparison of Color Combinations of the (a) Original TIMS imagery and the (b) Decorrelated TIMS Imagery Bands 6 (Blue), 3 (Green), and 2 (Red). In the original image some correlation was apparent, although gray shades dominate the scene. After the decorrelation procedure, a much greater range of colors was introduced. Note the resultant spectral differences of the buildings following the enhancements.

LR5) and DN 78 (i.e., LR2 and LR7). As a result of analyses by experienced photointerpreters, the four targets clustered around DN 137 were identified as two flat roofs covered with stones which appeared as light and dark green on the color infrared imagery (i.e., LR1 and LR3), and two metal rooftops, flat and gabled, which appeared as light and medium gray (i.e., LR4 and LR5). These four targets, made up of two very different materials, could not be distinguished in the simulated broad-band imagery. When the narrow-band thermal images were examined, however, differences became apparent. No complete separation was found between LR1 and LR3 in any of the bands, though none was expected because each target had the same orientation (i.e., flat) and was made up of the same type of material (i.e., stones). However, the confusion between targets made up of different materials no longer existed; target LR4 was separated from LR1 in TIMS band 1 at the 95 percent confidence interval and TIMS bands 2 and 3 at 65 percent confidence interval. Target LR4 was not distinguishable from LR3 in any bands at the 95 percent confidence interval. Target LR5 was separable from LR1 in bands 2 and 3 at 95 percent and 5 and 6 at the 65

TABLE 5. CORRELATION MATRICES FOR THE ORIGINAL, PRINCIPAL COMPONENT, AND DECORRELATION-STRETCHED TIMS DATA SET. THESE CORRELATIONS WERE CALCULATED BASED ON 2801 PIXELS REPRESENTING A VARIETY OF COVER TYPES.

			Original Bands		
	1	2	3	4	6
1	1.0000				
2	0.9668	1.0000			
3	0.9088	0.9632	1.0000		
4	0.9292	0.8495	0.7466	1.0000	
6	0.8751	0.7756	0.6589	0.9810	1.0000
			Principal Component Bands		
	1	2	3	4	5
1	1.0000				
2	0.1420	1.0000			
3	−0.3572	−0.3892	1.0000		
4	0.5024	0.2107	−0.2913	1.0000	
5	0.3711	0.4997	−0.3456	0.2742	1.0000
			Decorrelation-Stretched Bands		
	1	2	3	4	6
1	1.0000				
2	0.1420	1.0000			
3	−0.3572	0.6860	1.0000		
4	0.5024	−0.2364	−0.2186	1.0000	
6	0.3711	−0.5115	−0.6150	0.8238	1.0000

TABLE 6. LITTLE ROCK: STATISTICAL MEANS AND STANDARD DEVIATIONS FROM TRAINING AREAS (BUILDINGS) IN THE SIMULATED BROAD-BAND IMAGE AND THE ORIGINAL IMAGERY WITH A LINEAR STRETCH APPLIED. BAND 5 IS INCLUDED FOR COMPARISON; HOWEVER, IT WAS NOT USED IN THE STUDY. LR1 AND LR3 WERE FLAT ROOFS COVERED WITH STONES. LR4 WAS A FLAT METAL ROOF, AND LR5 WAS A GABLED METAL ROOF. LR2 AND LR7 WERE GABLED AND LIKELY METAL. THE TARGET DESCRIPTION REFERS TO THE COLOR OF THE ROOFING MATERIAL AS IT APPEARED IN THE COLOR INFRARED PHOTOGRAPHY.

Target Description		1	2	3	4	5	6	Simulated Broad-Band
LR1	MEAN:	102.06	94.94	73.71	113.17	123.31	128.09	143.06
Flat Green	STD:	5.26	4.74	6.76	4.91	4.60	4.76	6.31
LR2	MEAN:	66.53	65.99	51.60	53.06	39.74	31.94	69.31
Gable Gray	STD:	2.26	2.42	3.34	3.73	3.99	4.42	4.14
LR3	MEAN:	92.71	88.33	65.03	105.05	115.45	121.08	132.26
Flat Green	STD:	4.87	4.65	6.49	3.65	3.48	4.55	5.85
LR4	MEAN:	82.85	81.82	57.21	106.80	118.00	121.87	127.77
Flat Gray	STD:	4.72	4.68	6.28	3.77	3.89	4.31	5.62
LR5	MEAN:	109.54	112.71	106.69	107.87	109.35	111.62	148.08
Gable Gray	STD:	3.40	2.64	3.12	2.84	4.44	5.76	4.71
LR7	MEAN:	63.27	77.86	68.82	70.97	56.51	49.54	86.91
Gable Gray	STD:	5.12	4.44	5.41	5.30	6.62	7.24	7.41

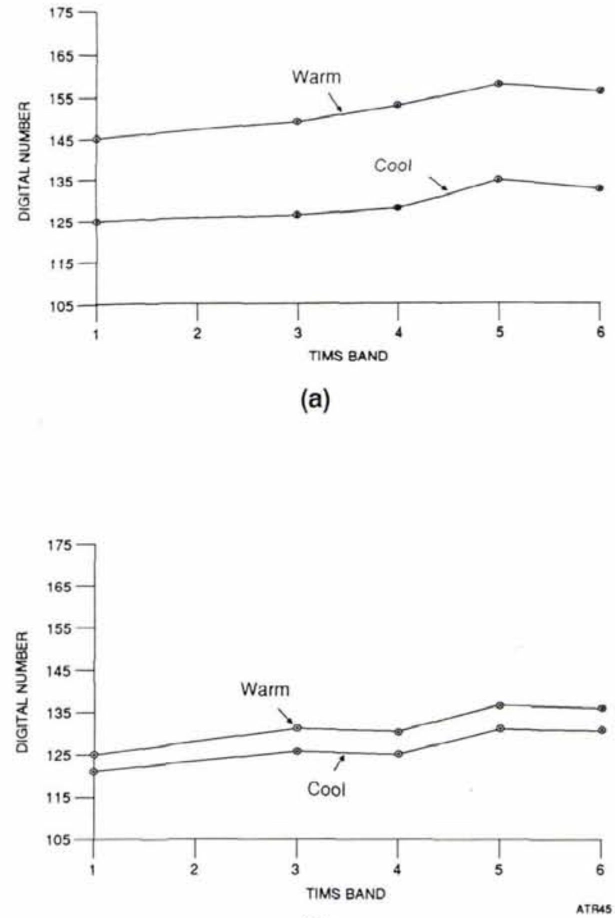

FIG. 2. Plots of digital numbers after linear stretching versus TIMS band number from "warm" and "cool" portions of two gabled roofs: (a) Building 1, and (b) Building 2. The similarities between these curves taken from the same roofing material type suggested that, while different orientations may yield different temperatures, the characteristic shape of the spectral curves may help identify specific objects.

percent confidence interval. Target LR5 was separable from LR3 in bands 1, 2, and 3 at the 95 percent interval and also band 6 at the 65 percent confidence interval.

To compliment the above results, statistics were generated from TIMS imagery for another location. The second TIMS data set was acquired over Fort Polk, Louisiana two hours prior to the Little Rock data set (i.e., at midnight). These data were utilized because they included buildings with gabled roofs having both east and west orientations. Plots were generated for the two different aspects of the same rooftops. Two rooftops were selected and measurements were made on "warm" and "cool" sides of each (i.e., one side had faced the sun more recently than the other). This was done to examine the spectral signature of the same material at different temperatures. Figures 2a and 2b show the digital numbers of these warm and cool target regions plotted against TIMS band number. Of particular significance was the similarity between the spectral curves of the same material at the two different temperatures. This suggested that, although similar objects may have different temperatures due to differences in orientation, the characteristic shape of the spectral curves may be used to help identify the objects in question. Similarly, returning to the Little Rock data, Figure 3 shows the spectral curves of two of the flat, stone-covered roofs (differences probably due to different roofing materials because aspects were the same). Note how similar the spectral curves of the two roofs are to one another and, in particular, how different they are from the gabled roofs (Figures 2a and 2b).

In summary, both of the metallic roofs were confused with both of the stone-covered roofs in the broad-band image at the 95 percent confidence interval. The two groups, however, were separable using the narrow-band images at the 95 percent level with the exception of LR3 and LR4. The separation of LR3 and LR4 is reexamined in later paragraphs. Even though temperatures varied for the same roofing material due to aspect, over

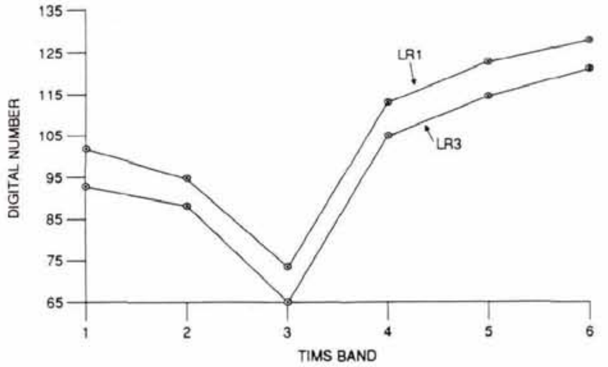

FIG. 3. Plotted spectral curves (digital number after linear stretching versus TIMS band number) of two flat, stone-covered roofs: buildings LR1 and LR3. In this example, because the aspects were the same, differences in digital number were probably due to slightly different roofing materials. Note, however, how similar the spectral curves were to each other and how different they were from the gabled roofs in Figures 2a and 2b.

the full spectral range, there were characteristic spectral curves associated with specific roofing materials.

SUMMARY AND CONCLUSIONS

Using the multispectral TIMS imagery collected at night, visual and statistical analyses have shown that manmade and natural objects could be more easily differentiated using multi-band (i.e., narrow band) thermal infrared data as opposed to simulated broad-band thermal imagery. This was evident even though the six TIMS bands were highly correlated. Furthermore, to study the problems associated with false-alarms, the utility of the TIMS imagery was increased through the use of a decorrelation-stretch technique which involved generating principal component (PC) images, applying a contrast stretch, and performing an inverse transformation. It was found that the Gaussian stretch was generally a better overall enhancement; however, in some cases, fine detail (i.e., subtle tonal differences) was lost with noise becoming more apparent. It was found that PC images 3, 4, and 5 were very noisy, although key information was located in these images. When the inverse transformation was performed, there was a dramatic noise reduction in the resultant imagery, particularly when a median filter was initially applied to the corresponding PC images.

Although small sample sizes were used, the utility of developing multispectral TIR capabilities for night reconnaissance applications was addressed. These initial research results indicated that further investigations using the discussed methodology are warranted.

ACKNOWLEDGMENT

This study was supported by the Department of the Army, Center for Night Vision and Electro-Optics, Fort Belvoir, Virginia. The authors are grateful for the support and consultations provided by Joseph Swistak, Chief, Multi-Sensor Acquisition Techniques Team at the Center for Night Vision and Electro-Optics, Fort Belvoir, Virginia.

REFERENCES

Gillespie, A. R., 1986. Enhancement of TIMS Images for Photointerpretation. *The TIMS Data User's Workshop*, (A. B. Kahle and E. Abbott, eds.) 18–19 June 1985, JPL Publication 86-38, Pasadena, Calif., Jet Propulsion Laboratory, pp. 12–24.

Gillespie, A. R., A. B. Kahle, and R. E. Walker, 1986. Color Enhancement of Highly Correlated Images. *Remote Sensing of Environment, Decorrelation and HSI Contrast Stretches*, 20:209–235.

Gonzalez, R. C., 1986. Image Enhancement and Restoration: *Handbook of Pattern Recognition and Image Processing*, (T.Y. Yang and K. S. Fu, eds.) Academic Press, pp. 191–213.

Palluconi, F. D., and G. R. Meeks, 1985. *Thermal Infrared Multispectral Scanner (TIMS): An Investigator's Guide to TIMS Data*, JPL Publication 85-32, Pasadena, Calif., Jet Propulsion Laboratory, 22 p.

Putnam, E. S. (ed.), 1986. *Commercial Applications and Scientific Research Requirements for the Thermal-Infrared Observations of Terrestrial Surfaces*, NASA and EOSAT, 145 p.

Schott, J. R., 1989. Image Processing of Thermal Infrared Images. *Photogrammetric Engineering & Remote Sensing*, Vol. 55, No. 9, pp 1311–1321.

Soha, J. M., and A. A. Schwartz. 1978. Multispectral Histogram Normalization Contrast Enhancement, *Proc. Fifth Canadian Symposium on Remote Sensing*, Victoria, B.C., Canada, pp. 86–93.

Swain, P. H., and S. M. Davis (eds.), 1978. *Remote Sensing: The Quantitative Approach*, McGraw-Hill Book Co., 396 p.

Taylor, M. M., 1973. Principal Components Color Display of ERTS Imagery, *Third Earth Resources Technology Satellite-1 Symposium*, NASA SP-351, Vol. 1, Section B, pp. 1877–1897.

(Received 13 September 1990; revised and accepted 12 March 1991)